A hybrid cyt *c* maturation system enhances the bioelectrical performance of engineered *Escherichia coli* by improving the rate-limiting step

Author List:

Lin Su [1,2,3], Tatsuya Fukushima [3], Caroline M. Ajo-Franklin [2,3,4,5*]

Author Affiliations:

[1] State Key Laboratory of Bioelectronics, School of Biological Science and Medical Engineering, Southeast University, Nanjing 210018, China

[2] Department of BioSciences, Rice University, Houston, TX 77005, USA

[3] Molecular Foundry, Lawrence Berkeley National Laboratory, Berkeley, CA 94720, USA

[4] Molecular Biophysics and Integrated Biosciences Division, Lawrence Berkeley National Laboratory, Berkeley, CA 94720, USA

[5] Institute for Biosciences and Bioengineering, Rice University, Houston, TX 77005, USA

* To whom correspondence should be addressed. Tel: 1-713-348-3497; Fax: 1-713-348-4790; Email: cajo-franklin@rice.edu

ABSTRACT

Bioelectronic devices can use electron flux to enable communication between biotic components and abiotic electrodes. We have modified *Escherichia coli* to electrically interact with electrodes by expressing the cytochrome *c* from *Shewanella oneidensis* MR-1. However, we observe inefficient electrical performance, which we hypothesize is due to the limited compatibility of the *E. coli* cytochrome *c* maturation (Ccm) systems with MR-1 cytochrome *c*. Here we test whether the bioelectronic performance of *E. coli* can be improved by constructing hybrid Ccm systems containing protein domains from both *E. coli* and *S. oneidensis* MR-1. The hybrid CcmH increased cytochrome *c* expression by increasing the abundance of CymA 60%, while only slightly changing the abundance of the other cytochromes *c*. Electrochemical measurements showed that the overall current from the hybrid *ccm* strain increased 121% relative to the wildtype *ccm* strain, with an electron flux per cell of 12.3 ± 0.3 $fA \cdot cell^{-1}$. Additionally, the hybrid *ccm* strain doubled its electrical response with the addition of exogenous flavin, and quantitative analysis of this demonstrates CymA is the rate-limiting step in this electron conduit. These results demonstrate that this hybrid Ccm system can enhance the bioelectrical performance of the cyt *c* expressing *E. coli*, allowing the construction of more efficient bioelectronic devices.

KEYWORDS

Microbial electrochemistry, microbial fuel cell, bioelectronic sensor, synthetic biology, cytochrome *c* maturation

37 **1. INTRODUCTION**

38 The flow of electrons can transfer both energy and information between living and non-living
39 systems for bioelectronic and biosensing applications. Extracellular electron transfer (EET)
40 pathways (Shi et al., 2016) can electrically connect living microorganisms with electrochemical
41 cells, enabling applications such as power generation in microbial fuel cells (MFCs) (Gul and
42 Ahmad, 2019; Logan, 2009; Santoro et al., 2017; Slate et al., 2019) and environmental sensing in
43 bioelectronic sensing systems (Chouler et al., 2018; Wang et al., 2013; Zhou et al., 2017).
44 Engineering EET in native electroactive microorganisms, such as *Shewanella oneidensis* MR-1
45 (Cheng et al., 2020; Min et al., 2017; West et al., 2017), and non-native hosts, such as *Escherichia*
46 *coli* (Jensen et al., 2016; Sturm-Richter et al., 2015; Thirumurthy and Jones, 2020) or
47 *Pseudomonas putida* (Schmitz et al., 2015), has expanded the range of potential applications
48 (Harris et al., 2017; Su and Ajo-Franklin, 2019). However, a fundamental limitation in these
49 bioelectronic systems is the low rate of EET, which causes these devices to have low power output,
50 low sensing sensitivity, and limited robustness. For example, expressing the EET pathway from
51 *Shewanella oneidensis* MR-1 into engineered *E. coli* only yields ~10% the current produced by
52 MR-1 (TerAvest et al., 2014).

53 The molecular structure of these EET pathways is increasingly well-understood. The direct EET
54 pathways (Mtr pathway) in *Shewanella oneidensis* MR-1 is a group of multiheme cytochrome *c*
55 (cyt *c*) proteins embedded in the inner membrane (CymA), in the periplasm (Stc, FccA), and outer
56 membrane (MtrC, MtrA) (Clarke et al., 2011; Okamoto et al., 2011; Rosenbaum et al., 2012). We
57 and others (Jensen et al., 2016; Su et al., 2020; TerAvest et al., 2014) have found that expressing
58 the CymA, MtrC, MtrB and MtrA proteins of the Mtr pathway enables *E. coli* to perform EET
59 (**Figure 1A**).

Expressing the Mtr cyt *c* proteins requires the cytochrome *c* maturation (Ccm) system, which covalently ligates heme *b* groups to the apo-cyt *c* protein to form the holo-cyt *c* (Sanders et al., 2010; Verissimo et al., 2011). The Ccm systems of α- and β-proteobacteria contains three modules (**Figure 1B**): the heme *b* translocation module that conveys heme *b* into the periplasm and to the ligation module, the apo cyt *c* chaperone module that maintains apocyt *c* in the reduced state, and the ligation module that catalyzes formation of a thioether bond between the heme b and apocyt *c* (Kranz et al., 2009; Sanders et al., 2010; Thöny-Meyer, 2000). In both *S. oneidensis* and *E. coli*, CcmA, B, C, D and E form the heme delivery module, and CcmG and DsbD compose the chaperone module. While *E. coli* uses two proteins, CcmF and CcmH, as the ligation module, this module in *S. oneidensis* MR-1 includes a third protein - CcmI (**Figure S1**). We recently found that mutations in the C-terminal domain of CcmH can significantly change the EET efficiency by changing the stoichiometry of the Mtr cyt *c (Su et al., 2020)*. This finding suggested that optimizing the heme ligation process by redesigning CcmH of *E. coli* could remodel the stoichiometry of cyt *c* and enhance the bioelectrical performance of Mtr-expressing *E. coli*.

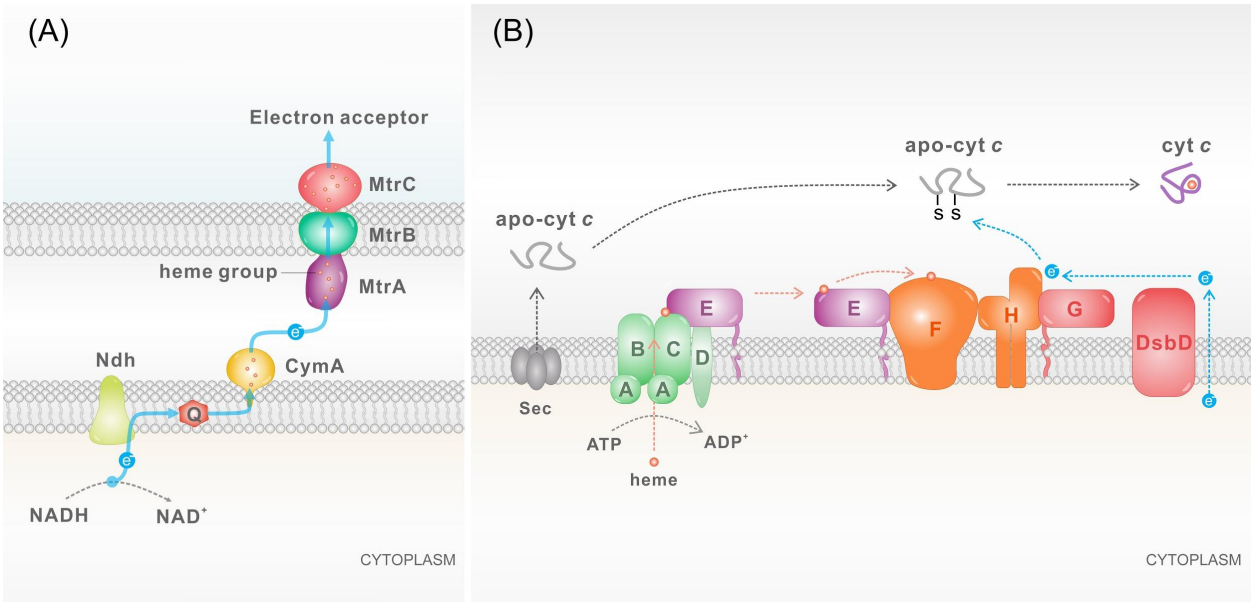

75

76 **Figure 1. A schematic of the Mtr pathway in engineered *E. coli* and the three modules of**
77 **Ccm system in *E. coli*.** (A) The Mtr pathway includes MtrC, MtrB, MtrA and CymA from
78 *Shewanella oneidensis* MR-1, which enable engineered *E. coli* to perform extracellular electron
79 transfer. (B) For cytochrome *c* (cyt *c*) such as MtrC, MtrA and CymA to mature, the Ccm system
80 catalyzes ligation of heme with apo-cyt *c* to form covalent bonds with heme groups. In *E. coli*, the
81 Ccm system is composed of eight different Ccm proteins, CcmA, B, C, D, E, F, G, H, and a DsbD
82 (disulfide bond formation protein). These proteins form three functional modules: heme delivery
83 (green and purple), apo cyt *c* chaperone (red), and ligation (orange).

84 The role of the C-terminal domain of CcmH in cyt *c* maturation is disputed. Fabianek et al.
85 (Fabianek et al., 1999) and Robertson et al. (Robertson et al., 2008) demonstrated that *E. coli*
86 strains with an incomplete CcmH lacking its C-terminal domain can still mature both the native
87 diheme cyt *c* (NapB) and a heterologous monoheme cyt *c* (Cyt *c* C550). They contend that the C-
88 terminal is not required for maturation because of functional redundancy between the two domains
89 of CcmH. In contrast, Zheng et al. (Zheng et al., 2012) predicted the C-terminal of CcmH is a TRP
90 (tetratricopeptide repeat) -like domain which recognizes apo-cyt *c* and concluded it is essential for
91 cyt *c* expression. Our previous results suggest the C-terminal of CcmH is essential in expressing
92 multi-heme heterologous cyt *c* (Su et al., 2020), agreeing more closely with Zheng et al. (Zheng et
93 al., 2012).

94 To optimize the heme ligation process for Mtr cyt *c*, here we constructed a hybrid CcmH that
95 uses protein domains from *E. coli* (the N-terminal of CcmH) and *S. oneidensis* MR-1 (the C-

96 terminal of CcmI). We then explored the effects on cyt *c* expression and EET efficiency to test if
97 this hybrid CcmH could boost the bioelectrical performance of Mtr-expressing *E. coli*.

98

99 **2. METHODS**

100 **2.1 Construction of *E. coli* strains with *ccm* variants**

101 We used Phusion DNA polymerase (NEB) for all the PCR amplification (please refer to
102 Supplementary Information for cloning procedures). We have listed all the primers, plasmids, and
103 strains we used in Table S1 and S2. We sequence-verified all plasmids used and transformed them
104 into the *E. coli* C43(DE3) background (Lucigen) to construct all the strains.

105 **2.2 Cyt *c* expression and growth conditions for *E. coli* strains**

106 To express cyt *c*, we first inoculated all the *E. coli* strains directly from -80 °C glycerol stocks in
107 5 mL LB media with antibiotics (50 μg/mL kanamycin and 34 μg/mL chloramphenicol) and grew
108 them at 37 °C overnight with 250 rpm sharking. Then we inoculated cell cultures (1:100 v/v ratio)
109 in 50 mL 2xYT media in foil-covered 250 mL flasks with the same antibiotic concentrations and
110 1 mM δ-ALA (aminolevulinic acid), and grew these cultures at 37 °C with 250 rpm sharking.
111 When the cell OD_{600} reached between 0.5 to 0.6, we added 4 μM IPTG to induce the expression
112 of cyt *c*, followed by culturing at 30 °C with 250 rpm shaking overnight. Then we washed cells
113 twice with M9 minimal medium (BD). All the chemicals and media are from Sigma-Aldrich unless
114 otherwise noted.

115 **2.3 Redness screening of the *E. coli* strains with *ccm* variants**

116 We used redness screening for detecting the overall expression level of cyt *c*, as previously
117 described (Su et al., 2020). We first grew all the strains from -80 °C glycerol stocks, then inoculated
118 cell cultures in 2xYT media with foil-covered flasks (see **section 2.2**). When the cell OD_{600} reached
119 between 0.5 to 0.6, we split the cell cultures into 96-well deep-well plates (Polypropylene 2.2 mL,
120 VWR), where each well contained 0.5 mL cell culture. We then induced the cells with a gradient
121 concentration of IPTG (0, 0.5, 1, 2, 4, 8, 16, 32, 62.5, 125, 250, and 500 μM). After overnight
122 incubation, we transferred the cell cultures into 96-well white round-bottom microplates (3789A,
123 Corning), and centrifuged the plate to pellet the cells. After removing the media, we used a scanner
124 to take pictures of the plates and measured the redness of the cell pellets with a MATLAB image
125 processing program (Su et al., 2020).

126 **2.4 Enhanced chemiluminescence measurement of cyt *c* expression**

127 We used enhanced chemiluminescence (ECL) to detect the cyt *c* expression as previously
128 described (Su et al., 2020). In brief, we mixed 20 μL of 10 OD_{600} washed cells (described in **2.1**)
129 with an equal volume of Laemmli Sample Buffer (2x), and heated the mixture to 95°C for 15 min.
130 Then we loaded the samples and protein ladder (Precision Plus Protein WesternC Standards) into
131 an SDS-gel (4-20% Crit TGX Stain-Free Gel) to perform SDS-PAGE (160 V, 45 min). Next, we
132 transferred proteins from the SDS-gel onto the nitrocellulose membrane (Trans-Blot Turbo Midi
133 NC Transfer Packs) via the Trans-Blot Turbo Transfer System (Bio-Rad). We then used ECL kit
134 (Pierce Pico West Enhanced Chemiluminescence substrate, ThermoFisher) to perform the cyt *c*
135 detection assay. Finally, we imaged the ECL signals using the FluorChem E system
136 (ProteinSimple). All the chemicals and supplies are from Bio-Rad unless otherwise indicated.

137 **2.5 Bioelectrochemical measurement**

138 We used two-chamber, three-electrode electrochemical reactors to perform the electrochemical
139 experiments as previously described (Su et al., 2020). The reactors contained three electrodes: a
140 working electrode (graphite felt, Alfa Aesar) and a reference electrode (CHI111, Ag/AgCl with 3
141 M KCl, CH Instruments) in the anodic chamber, and a counter electrode (titanium wire, Alfa
142 Aesar) in the cathodic chamber. We also used a cation exchange membrane (CMI-7000S,
143 Membranes International) to separate these two chambers. Each chamber contained 150 mL M9
144 minimal medium (BD) and 50 mM D,L-lactate (Sigma-Aldrich) as the electrolyte. During the test,
145 we continuously purged the anodic chamber with N_2 gas to maintain anaerobic conditions, and we
146 kept the temperature at 30 °C by placing all the reactors in an incubator. We used a potentiostat
147 (VSP-300, Bio-Logic Science Instruments) to perform all the electrochemical measurements. We
148 set the applied potential at 0.2 V versus the reference electrode to conduct chronoamperometry,
149 and the electrical current (averaged at every 36 s) is reported as a function of the geometric surface
150 area of the working electrode (0.0016 m^2, two sides, diameter of 32 mm). For the differential pulse
151 voltammetry (DPV) measurement (Xu et al., 2016), we scanned the potential from -0.4 V to 0.2 V
152 versus the reference electrode, with the pulse height set to 50 mV, pulse width set to 500 ms, step
153 height set to 1.0 mV, and step time set to 1000 ms.

154 **3. RESULTS AND DISCUSSION**

155 **3.1 Design and construction of a hybrid cyt *c* maturation operon in *Escherichia coli***

156 To test our hypothesis that MR-1's ligation module is more efficient at maturing MR-1 cyt *c* than
157 *E. coli*'s ligation module, we made a series of modifications to the *ccmH* gene in the plasmid which
158 carries the *ccm* operon from *E. coli* (**Figure 2**). We then co-transformed these plasmids with a

159 separate plasmid that expresses *cymAmtrCAB* from MR-1 into *E. coli* C43(DE3) to create the
160 wildtype *ccm*, *ccmHI*, *ccmH*^{N}, and hybrid *ccmH* strains (**Table 1**). Specifically, to test the effect
161 of altering the entire ligation module, we replaced *ccmH* from *E. coli* with *ccmHI* from MR-1,
162 creating the I5101 plasmid in the *ccmHI* strain. To test the impact of replacing only the apo cyt *c*
163 binding component, we fused the N-terminal region of the *E. coli ccmH* with the C terminal region
164 of MR-1 *ccmI*, notated as the I5099 plasmid in hybrid *ccmH* strain. As a control, we also made the
165 I5100 plasmid in *ccmH*^{N} strain from the I5099 plasmid, in which the C-terminal domain of *S.*
166 *oneidensis* CcmI was removed. We also constructed a strain with the pACYC184 empty vector
167 and *cymAmtrCAB* plasmid, dubbed the 'no *ccm*' strain, as a negative control.

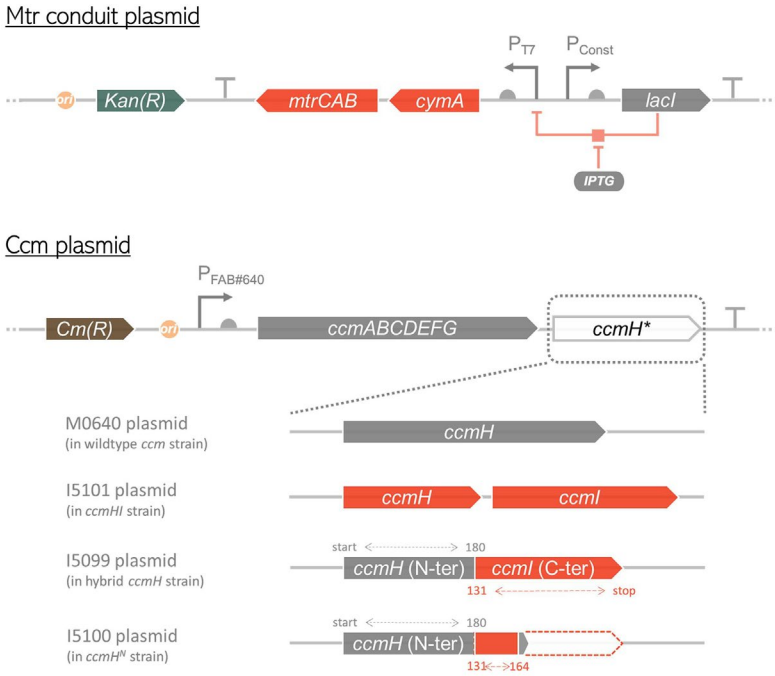

168

169

170 **Figure 2. A schematic illustration describing the two plasmids we used for cytochrome *c***
171 **expression in engineered *E. coli*.** For the Mtr conduit plasmid, *cymA*, *mtrC*, *mtrA*, *mtrB* are under

172 the same T7 lacO promoter (P_{T7}); for the Ccm plasmid, all the components are under a constitutive
173 promoter ($P_{FAB\#640}$). In the Ccm plasmid, we replaced the coding sequence of *ccmH* from the *E.*
174 *coli ccm* operon with three other variants. These plasmids coded for CcmHI from MR-1 (I5101),
175 a fusion between the N terminal region of *E. coli ccmH* and the C terminal region of CcmI from
176 MR-1 (I5099), and a control that removed the C terminal region of MR-1 CcmI (I5100). Gray and
177 red regions indicate DNA regions that code for proteins from *E. coli* and MR-1, respectively. (ori
178 origin of replication; promoter; ribosome-binding site, RBS; coding sequence, CDS; T
179 terminator).

180 **Table 1. Strains Used in This Study**

Strain Name	Parental Strain	Plasmid(s)	Genes*	Source
wildtype *ccm*	C43(DE3)	M0640	*ccmABCDEFGH*	(Goldbeck et al., 2013)
		I5049	*cymA, mtrCAB*	(Jensen et al., 2016)
hybrid *ccm*	C43(DE3)	I5099	*ccmABCDEFG, hybrid ccmH*	this work
		I5049	*cymA, mtrCAB*	(Jensen et al., 2016)
$ccmH^N$	C43(DE3)	I5100	*ccmABCDEFG, ccmH (N-term.)*	this work
		I5049	*cymA, mtrCAB*	(Jensen et al., 2016)
ccmHI	C43(DE3)	I5101	*ccmABCDEFG,* $ccmHI_{SO}$	this work
		I5049	*cymA, mtrCAB*	(Jensen et al., 2016)
no *ccm*	C43(DE3)	pACYC184	Empty plasmid vector (no *ccm*)	

I5049	*cymA, mtrCAB*	(Jensen et al., 2016)

181 * Details of the genes are available in supporting information, Table S2.

182 **3.2 The hybrid Ccm system can increase cyt *c* abundance in *E. coli***

183 To test if these *ccm* variants can mature and change the cyt *c* expression level, we first examined
184 the cyt *c* expression of these *E. coli* strains with a redness assay (Su et al., 2020) across different
185 IPTG induction levels (**Figure 3**). Since IPTG induction level is non-linear with protein
186 expression, we present this data in term of relative promoter strength, which is the GFP expression
187 per cell at a IPTG concentration normalized by the maximal GFP expression per cell (Goldbeck et
188 al., 2013). The redness value, which indirectly measures the cyt *c* per cell, peaked at the relative
189 promoter strength of ~ 0.1 (arb. strength units) for all the strains with a Ccm plasmid. As expected,
190 the no *ccm* strain has the lowest redness value because it cannot mature cyt *c,* and the wildtype
191 *ccm* strain has a high redness value, consistent with its ability to mature cyt *c*. Compared to the
192 wildtype *ccm* strain, the redness value of the *ccmHI* strain decreased by ~40% (0.15 ± 0.003 arb.
193 red units in *ccmHI* vs. 0.25 ± 0.003 arb. red units in wildtype). This decrease in cyt *c* expression
194 might be due to a poor ability of the *E. coli* and MR-1 proteins to form a functional complex
195 (Zheng et al., 2012). In contrast, the hybrid *ccmH* strain has a redness value (0.27 ± 0.002 arb. red
196 units) that is 8% greater than the wildtype *ccm* strain, indicating that it can mature cyt *c* slightly
197 better. This robust cyt *c* expression shows the C terminal region of CcmI from MR-1 can
198 functionally replace the C terminal region of *E. coli* CcmH. Overall, these data show that the hybrid
199 *ccm* system can increase cyt *c* abundance in *E. coli*, which potentially may increase its EET
200 efficiency.

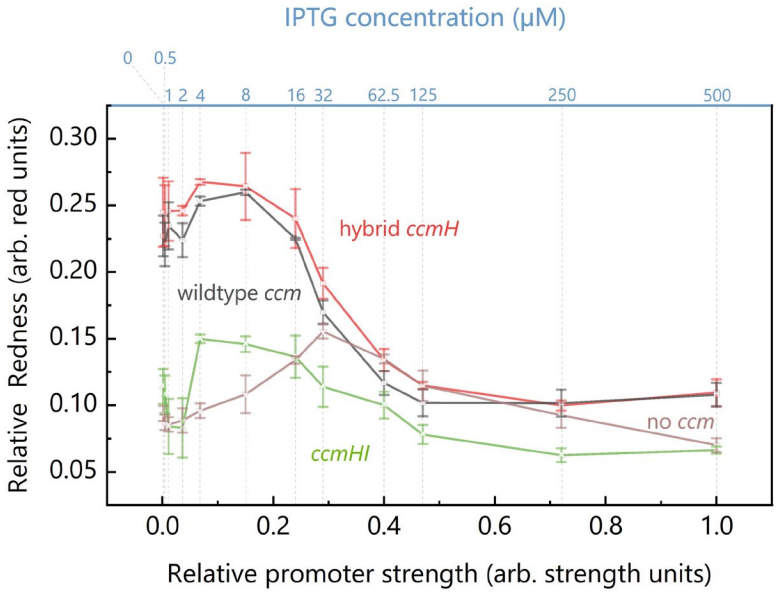

Figure 3. The hybrid *ccmH* strain expresses more cytochromes *c*. Relative redness as a function of relative promoter strength, i.e., induction level, for *E. coli* expressing *cymAmtrCAB* with different *ccm* operons. The hybrid *ccmH* strain has a higher level of overall cyt *c* expression than wildtype *ccm* strain. Results are representative of three independent experiments.

3.3 The hybrid Ccm system changes Mtr cyt *c* stoichiometry

To further investigate how the hybrid *ccm* system alters the expression of cyt *c* in the Mtr pathway, we used enhanced chemiluminescence (ECL) to characterize the abundance of CymA, MtrC, and MtrA in hybrid *ccmH* strain, wildtype *ccm* strain, and no *ccm* strain (**Figure S2**). These strains were all induced at 0.068 arb. strength units relative promoter strength (4 μM IPTG) since the hybrid *ccm* strain has one of the highest cyt *c* expressions at this induction (**Figure 3**). As expected, there was no detectable amount of cyt *c* in the no *ccm* strain (**Figure S2**). While the MtrC abundance was very similar, the abundance of MtrA decreased ~15%, and CymA increased ~60% in the hybrid *ccm* strain relative to the wildtype *ccm* strain (**Figure 4**). These data show that

215 the hybrid *ccm* system increases the overall cyt *c* abundance by increasing the maturation of
216 CymA.

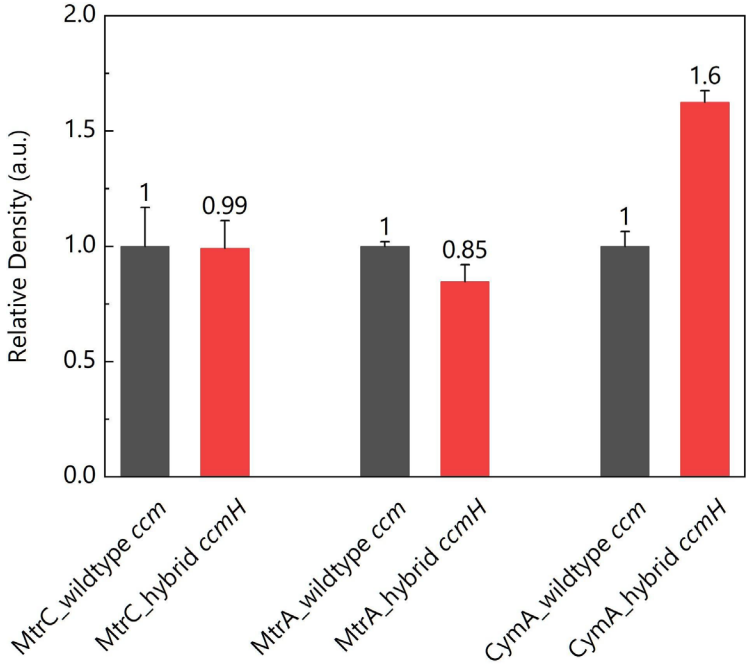

217

218

219 **Figure 4. The hybrid *ccm* system increases the CymA expression in *E. coli*.** The relative density
220 of enhanced chemiluminescence (ECL) bands arising from three cyt *c* heterologously expressed
221 in the hybrid *ccm* and wildtype *ccm* strains. The cyt *c* expression in negative control no *ccm* strain
222 was below the limit of detection. Results are representative of three independent experiments.

223 **3.4 The hybrid Ccm system increases the current generation of Mtr-expressing *E. coli***

224 Altering the stoichiometry of Mtr cyt *c* in *E. coli* can negatively or positively affect its
225 bioelectrochemical performance (Su et al., 2020). To probe if the increase of CymA expression in
226 hybrid *ccmH* strain will also enhance its bioelectrical performance, we measured the current
227 generation (**Figure 5**) by the wildtype *ccm*, hybrid *ccmH*, $ccmH^N$ strains in three-electrode

228 electrochemistry bioreactors. The wildtype *ccm* strain produced 11.47 ± 0.19 mA/m^2, in line with
229 our previous observations (Su et al., 2020). The hybrid *ccmH* strain produced 25.32 ± 3.61mA/m^2,
230 a 121% increase in current over the wildtype *ccm* strain. The *ccmH*^{N} strain produced only 3.42 ±
231 0.44 mA/m^2, about a 70% decrease relative to the wildtype *ccm* strain, similar to the no *mtr* strain
232 previously reported (TerAvest et al., 2014). Thus, we conclude that the hybrid *ccmH* strain matures
233 more CymA and produces higher current than the *E. coli* Ccm system.

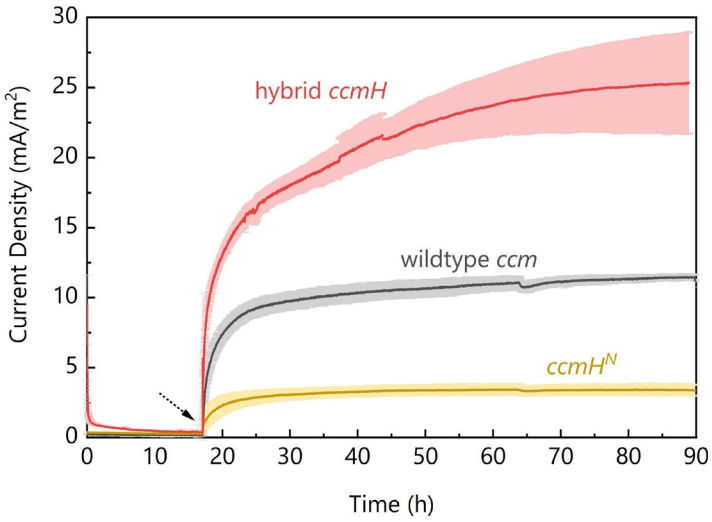

234

235

236 **Figure 5. The hybrid *ccmH* strain produces a higher current.** The current generation measured
237 by chronoamperometry in the bioreactors showing hybrid *ccmH* strain produces more current than
238 the wildtype *ccm* strain, while the negative control strain *ccmH*^{N} produces less current. Results are
239 representative of three independent experiments. The dotted arrow shows the time the bacteria
240 were injected.

241 To probe the mechanism underlying the increase in current production by the hybrid *ccmH* strain,
242 we performed differential pulse voltammetry (DPV) (**Figure 6**) after strains reached the steady-

243 state current generation after 90 h chronoamperometry testing. We observed a single anodic peak
244 at redox potential (E_p) of +51 mV_{SHE} in all three strains, which has been previously assigned to the
245 MtrCAB complex (Okamoto et al., 2013). This observation confirms that all three strains use the
246 MtrCAB conduit for the current production. The peak height in hybrid *ccmH* strain reached 8.31
247 μA, about 118% higher than the 3.82 μA in wildtype *ccm* strain, while in the $ccmH^N$ strain, it was
248 only 0.09 μA, about 2% of the wildtype. The ratio of the peak height for the hybrid *ccm* strain
249 relative to the wildtype *ccm* strain (2.18) closely mirrors the ratio of steady-state current for these
250 strains (2.21), indicating the increase in steady-state current arises from an increase in the flux of
251 electrons through the MtrCAB complex. Thus, the hybrid *ccm* strain produces more current by
252 more effectively maturing CymA, boosting its relative abundance, and increasing the electron flux
253 through the MtrCAB conduit.

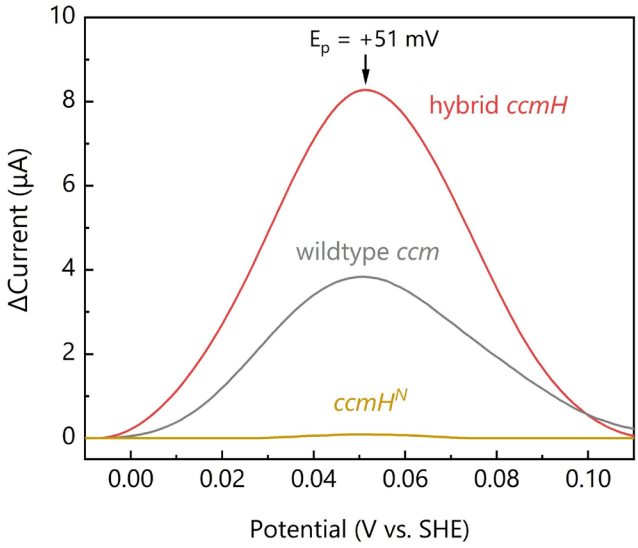

254

255 **Figure 6. The hybrid *ccmH* strain shows higher redox activity through cyt *c*.** Differential pulse
256 voltammetry (DPV) shows that the hybrid *ccmH* strain has a higher redox peak at the cyt *c* related
257 redox reaction potential (+51 mV vs. SHE). DPV signal smoothing and background deduction by
258 QSoas Version 2.0 (Fourmond et al., 2009).

259 **3.5 Hybrid *ccmH* strain produces more current per cell via both direct and indirect EET**

260 While DPV confirms that the increase in electron flux through the Mtr pathway increases the
261 current density, this increased flux could arise from an increase in the current per cell, an increase
262 in the number of viable cells, or an increase in both. To distinguish between these possibilities, we
263 measured both the current production and the number of viable cells using colony-forming unit
264 counting in the $ccmH^N$, hybrid *ccm*, and wildtype *ccm* strains (**Figure 7A**). The $ccmH^N$ strain
265 produced near baseline current on a per-cell basis (1.0 ± 0.005 fA·cell^{-1}), as expected. Interestingly,
266 the hybrid *ccmH* strains produced ~50% more current per cell than the wildtype *ccm* (12.3 ± 0.3
267 fA·cell^{-1} versus 8.3 ± 0.4 fA·cell^{-1}). These data confirm that the hybrid *ccmH* strain produces more
268 current at the single-cell level by direct EET.

269 In addition to direct EET via Mtr conduit, MR-1 (Brutinel and Gralnick, 2012; Coursolle et al.,
270 2010) can also perform EET with flavins as a bound cofactor to cyt *c* (Edwards et al., 2015;
271 Okamoto et al., 2014) or as a soluble mediator (Kotloski and Gralnick, 2013). To test if the hybrid
272 *ccmH* strain can also utilize flavin for EET, we added exogenous flavins and measured the current
273 density per cell. The addition of riboflavin to the $ccmH^N$ strain resulted in a meager current increase
274 (0.02 ± 0.004 fA·cell^{-1}·μM^{-1}). As expected, the current produced by both the wildtype *ccm* and
275 hybrid *ccm* strains linearly increased with the exogenous flavin concentration (**Figure 7A**).
276 However, the hybrid *ccm* strain produced significantly more current per μM exogenous flavin
277 (0.32 ± 0.06 fA·cell^{-1}· μM^{-1}) than the wildtype *ccm* strain (0.16 ± 0.01 fA·cell^{-1}·μM^{-1}) (**Figure**
278 **7A**). These data indicate that the hybrid *ccm* strain produces more current at the single-cell level
279 via a flavin-mediated EET as well as a direct EET mechanism.

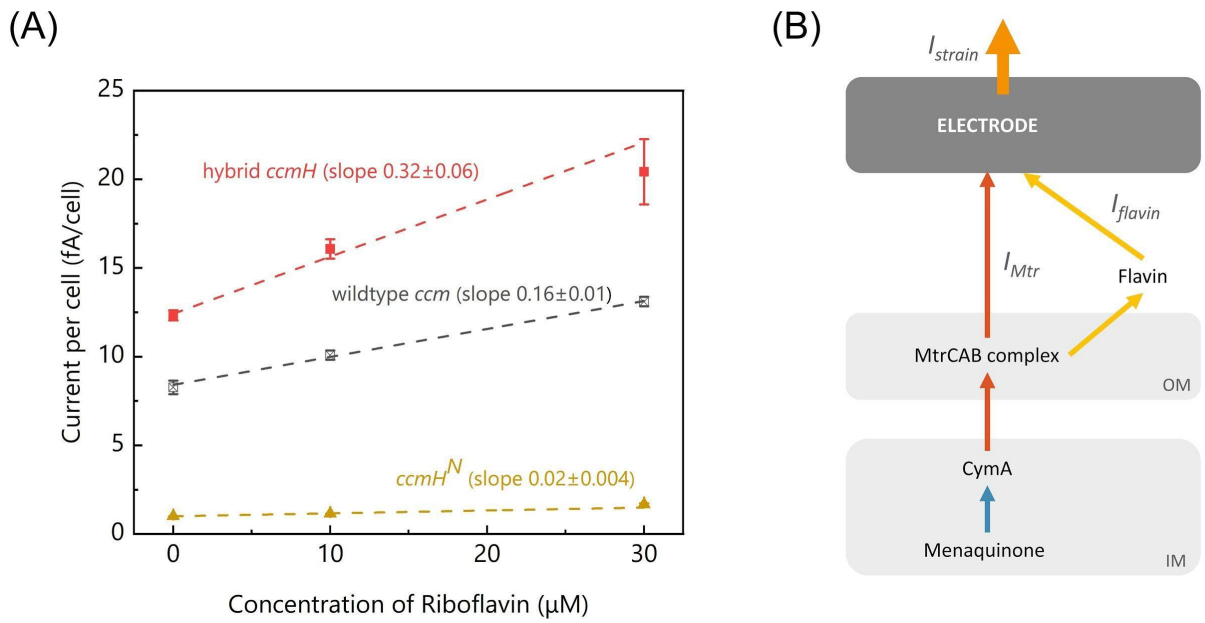

Figure 7. Current production by the hybrid *ccmH* strain is more sensitive to exogenous flavins. (A) The hybrid *ccmH* strain (red) has a more rapid and higher current response as a function of extra riboflavin concentration, compared to the wildtype *ccm* strain (gray), and $ccmH^N$ strain (yellow). Results are representative of two independent experiments. Linear fit analysis (with Y error) is performed by OriginPro 2019b (OriginLab Corporation). (B) A schematic depicting the extracellular electron transfer via Mtr conduit. MtrCAB complex receives the electrons from CymA, then delivers to the electrode (I_{strain}) through either MtrC (I_{Mtr}) or flavin (I_{flavin}). (OM: outer membranes, IM: Inner membranes).

3.6 Direct and flavin-mediated EET in the hybrid *ccmH* strain is limited by CymA

Our data suggest that the CymA amount limits electron flux and that the hybrid *ccmH* strain achieves higher current by enabling a greater electron flux from CymA into the same direct and

293 indirect EET routes found in the wildtype *ccm* strain. To quantitatively test these hypotheses, we
294 developed a quantitative model that relates EET in the hybrid *ccmH* strain to EET in the wildtype
295 *ccm* strain and then tested whether this model could explain the current per cell measurement in
296 the hybrid *ccmH* strain (**Figure 7**).

297 Explicitly, we modeled the overall EET current per cell (I_{strain}) as the sum of the direct EET via
298 Mtr conduit (I_{Mtr}) and flavin-mediated EET (I_{flavin}) (**Figure 7B**). We describe the flavin-mediated
299 EET as the product of the flavin concentration ($[flavin]$) and a constant of proportionality (k_{strain}),
300 (**Equation 1**):

301 $$I_{strain} = I_{strain,Mtr} + I_{strain,flavin} = I_{strain,Mtr} + k_{strain}[flavin] \quad (1)$$

302 Assuming the amount of CymA is rate-limiting in our system (**Figure 4**), we can then calculate
303 EET current in the hybrid *ccmH* strain (I_{hybrid}) as a ratio of the CymA concentration in the two
304 strains and the current in the wildtype *ccm* strain ($I_{WT,Mtr}$) with the equation below (**Equation 2**):

305 $$I_{hybrid} = \frac{[CymA]_{hybrid}}{[CymA]_{WT}} I_{WT} = \frac{[CymA]_{hybrid}}{[CymA]_{WT}} I_{WT,Mtr} + \frac{[CymA]_{hybrid}}{[CymA]_{WT}} k_{WT}[flavin] \quad (2)$$

306 Thus, both the intercept and slope of the best-fit line for the hybrid *ccm* strain should be equal to
307 the intercept and slope best-fit line of the wildtype *ccm* strain times the ratio of CymA
308 concentration in these two strains.

309 Using the experimentally-determined values of $I_{WT,Mtr}$ (8.3 ± 0.4 fA·cell^{-1}), k_{WT} (0.16 ± 0.01
310 fA·cell^{-1}·μM^{-1}), and $[CymA]_{hybrid}/[CymA]_{WT} = 1.6$, we can predict the values of I_{hybrid} and compare
311 it to our experimentally-determined values (**Figure 7A**). Both the predicted $I_{hybrid,\ Mtr}$ and $I_{hybrid,}$
312 $_{flavin}$ values, 13.28 ± 0.64 fA·cell^{-1} and 0.26 ± 0.02 fA·cell^{-1}·μM^{-1}, respectively, are quite close to

313 our observation of the direct EET (12.3 ± 0.3 fA·cell^{-1}) and mediated EET (0.32 ± 0.06 fA·cell^{-}
314 ^{1}·μM^{-1}) in hybrid *ccmH* strain. This result provides strong evidence that the hybrid *ccmH* strain's
315 improved bioelectrochemical performance arises mainly from the CymA expression increase and
316 underscores the importance of CymA in both direct EET and indirect EET.

317

318 **4. DISCUSSION**

319 In this study, we have shown that the C-terminal region of CcmH can be complemented by the
320 homologous region of CcmI from *S. oneidensis* MR-1, which increases the bioelectronic
321 performance of Mtr-expressing *E. coli*. We found that the hybrid CcmH can increase the overall
322 cyt *c* expression (**Figure 3**), with a preferred 60% increase in CymA expression (**Figure 4**). This
323 increase in CymA expression led to a 48% more EET current per bacterium and doubled the
324 electrical response to exogenous flavin (**Figure 7**), consistent with CymA being rate-limiting in
325 EET. In the following, we discuss how these findings impact the development of biofuel cells and
326 biosensors.

327 First, our data show that the C-terminal region of CcmH is essential for cyt *c*-based EET.
328 *Shewanella* and *Geobacter* species are the dominant organisms used for EET applications, such as
329 MFCs. These microorganisms express a significant amount of cyt *c* to perform EET (Meyer et al.,
330 2004; Shi et al., 2009). As a result, there are increasing efforts focused on genetically introducing
331 cyt *c* to make new organisms capable of EET (Schuergers et al., 2017; Sekar et al., 2016;
332 Thirumurthy and Jones, 2020), overexpressing cyt *c* to understand the structural basis of EET
333 (Edwards et al., 2020, 2019; Wang et al., 2019), and making cyt *c* -based conductive biomaterials
334 for bioelectrical applications (Liu et al., 2020; Sun et al., 2018). Previously we used a random

335 mutagenesis approach to improve cyt *c* maturation, which yielded strains that both increased
336 current by up to 77% and decreased current production by as much as -66% (Su et al., 2020).
337 Leveraging understanding from our previous study, this work presents a rational approach that
338 increased current by 121%. Thus, understanding how cyt *c* mature can provide guidance on
339 manipulating cyt *c* expression, which will assist both fundamental studies and these applied efforts
340 to increase the bioelectrical performance of MFCs.

341 Second, we found that the hybrid *ccmH* strain generates higher electrical signals using both Mtr
342 and flavin-mediated EET. Increasing the EET efficiency of Mtr-expressing *E. coli* is a particular
343 interest for biosensing because it can increase the signal-to-noise ratio, enabling higher sensitivity
344 detection. In recent years, much progress has been made in engineering the electrical
345 communication between bacteria and electrodes, such as responding to specific chemicals using
346 chemical-sensitive promoters (Golitsch et al., 2013; Webster et al., 2014; Yang et al., 2018),
347 miniaturized reactors with optimized structure design (Zhou et al., 2017), and modified material-
348 bacteria interface (Zajdel et al., 2018). Enhancing the bioelectrical performance of Mtr-expression
349 *E. coli* offers a reliable chassis in biosensing applications.

350 Lastly, our work provides guidance us on how to build a more efficient EET conduit for
351 bioelectrical sensing. Our model for the current generation in hybrid *ccmH* strain together with the
352 fact that CymA can only carry 40% (fewer heme groups per protein) as many electrons as MtrA
353 or MtrC, strongly suggests that electron transfer through CymA is a bottleneck for EET in the Mtr-
354 expression *E. coli*. Future work will focus on increasing the electron flux between menaquinone
355 and the MtrCAB complex to overcome this rate-limiting step. Also, since the electrical response
356 is linear in both CymA amount and flavin concentration, this informs more information rich
357 sensing scenarios, including building an "AND" gate with dual inputs.

358

359 **5. CONCLUSIONS**

360 In summary, a hybrid Ccm system altered the stoichiometry of the expressed cyt *c,* thus
361 accelerating the rate-limiting step in EET and enhancing the bioelectronic performance of *E. coli*.
362 Our results suggest that increasing the electron flux from menaquinone to MtrCAB complex could
363 further enhance the bioelectrical performance of engineered *E. coli*. More broadly, our work
364 provides a new strategy to express cyt *c* that underlies microbial bioelectronics and opens new
365 possibilities for engineering more sophisticated and sensitive biosensors.

366 **SUPPLEMENTARY DATA**

367 Supporting Information is available online.

368 **AUTHOR CONTRIBUTIONS**

369 L.S. contributed to strain construction, design of the study, conducting experiments, analysis of
370 the data, and writing and revision of the manuscript. T.F. contributed to strain construction, design
371 of the study, conducting experiments, analysis of the data, review and revision of the manuscript.
372 C.M.A-F. contributed to the design of the study, analysis of the data, and writing of the manuscript.

373 **ACKNOWLEDGMENT**

374 We thank Dr. Shuai Xu and Prof. Mohamed Y. El-Naggar, the University of Southern California
375 for discussions on the DPV experiments. Work at the Molecular Foundry was supported by the
376 Office of Science, Office of Basic Energy Sciences, of the U.S. Department of Energy [DE-AC02-

05CH11231]. This work was supported by the Office of Naval Research, [N0001418IP00037]; and the China Scholarship Council [201606090098 to L.S.].

379 **REFERENCES**

380 Brutinel, E.D., Gralnick, J.A., 2012. Appl. Microbiol. Biotechnol. 93, 41–48.
381 https://doi.org/10.1007/s00253-011-3653-0
382 Cheng, Z., Xiong, J., Min, D., Cheng, L., Liu, D., Li, W., Jin, F., Yang, M., Yu, H., 2020. Biotechnol.
383 Bioeng. 117, 1294–1303. https://doi.org/10.1002/bit.27305
384 Chouler, J., Cruz-Izquierdo, Á., Rengaraj, S., Scott, J.L., Di Lorenzo, M., 2018. Biosens. Bioelectron.
385 102, 49–56. https://doi.org/10.1016/j.bios.2017.11.018
386 Clarke, T.A., Edwards, M.J., Gates, A.J., Hall, A., White, G.F., Bradley, J., Reardon, C.L., Shi, L.,
387 Beliaev, A.S., Marshall, M.J., Wang, Z., Watmough, N.J., Fredrickson, J.K., Zachara, J.M., Butt,
388 J.N., Richardson, D.J., 2011. Proc. Natl. Acad. Sci. U. S. A. 108, 9384–9389.
389 https://doi.org/10.1073/pnas.1017200108
390 Coursolle, D., Baron, D.B., Bond, D.R., Gralnick, J.A., 2010. J. Bacteriol. 192, 467–474.
391 https://doi.org/10.1128/JB.00925-09
392 Edwards, M.J., Richardson, D.J., Paquete, C.M., Clarke, T.A., 2019. Protein Sci. 29, 830–842.
393 https://doi.org/10.1002/pro.3787
394 Edwards, M.J., White, G.F., Butt, J.N., Richardson, D.J., Clarke, T.A., 2020. Cell. 181, 665–673.
395 https://doi.org/10.1016/j.cell.2020.03.032
396 Edwards, M.J., White, G.F., Norman, M., Tome-Fernandez, A., Ainsworth, E., Shi, L., Fredrickson, J.K.,
397 Zachara, J.M., Butt, J.N., Richardson, D.J., Clarke, T.A., 2015. Sci. Rep. 5, 11677.
398 https://doi.org/10.1038/srep11677
399 Fabianek, R.A., Hofer, T., Thöny-Meyer, L., 1999. Arch. Microbiol. 171, 92–100.
400 https://doi.org/10.1007/s002030050683
401 Fourmond, V., Hoke, K., Heering, H.A., Baffert, C., Leroux, F., Bertrand, P., Léger, C., 2009.
402 Bioelectrochemistry 76, 141–147. https://doi.org/10.1016/j.bioelechem.2009.02.010
403 Goldbeck, C.P., Jensen, H.M., TerAvest, M.A., Beedle, N., Appling, Y., Hepler, M., Cambray, G.,

Mutalik, V., Angenent, L.T., Ajo-Franklin, C.M., 2013. ACS Synth. Biol. 2, 150–159. https://doi.org/10.1021/sb300119v

Golitsch, F., Bücking, C., Gescher, J., 2013. Biosens. Bioelectron. 47, 285–291. https://doi.org/10.1016/j.bios.2013.03.010

Gul, M.M., Ahmad, K.S., 2019. Biosens. Bioelectron. 142, 111576. https://doi.org/10.1016/j.bios.2019.111576

Harris, H.W., Sánchez-Andrea, I., McLean, J.S., Salas, E.C., Tran, W., El-Naggar, M.Y., Nealson, K.H., 2017. Front. Microbiol. 8, 2568. https://doi.org/10.3389/fmicb.2017.02568

Jensen, H.M., TerAvest, M.A., Kokish, M.G., Ajo-Franklin, C.M., 2016. ACS Synth. Biol. 5, 679–688. https://doi.org/10.1021/acssynbio.5b00279

Kotloski, N.J., Gralnick, J.A., 2013. mBio. 4, e00553-12. https://doi.org/10.1128/mbio.00553-12

Kranz, R.G., Richard-Fogal, C., Taylor, J.-S., Frawley, E.R., 2009. Microbiol. Mol. Biol. Rev. 73, 510–528. https://doi.org/10.1128/MMBR.00001-09

Liu, X., Gao, H., Ward, J.E., Liu, X., Yin, B., Fu, T., Chen, J., Lovley, D.R., Yao, J., 2020. Nature. 578, 550–554. https://doi.org/10.1038/s41586-020-2010-9

Logan, B.E., 2009. Nat. Rev. Microbiol. 7, 375–381. https://doi.org/10.1038/nrmicro2113

Meyer, T.E., Tsapin, A.I., Vandenberghe, I., de Smet, L., Frishman, D., Nealson, K.H., Cusanovich, M.A., van Beeumen, J.J., 2004. OMICS 8, 57–77. https://doi.org/10.1089/153623104773547499

Min, D., Cheng, L., Zhang, F., Huang, X.-N., Li, D.-B., Liu, D.-F., Lau, T.-C., Mu, Y., Yu, H.-Q., 2017. Environ. Sci. Technol. 51, 5082-5089. https://doi.org/10.1021/acs.est.6b04640

Okamoto, A., Hashimoto, K., Nealson, K.H., Nakamura, R., 2013. Proc. Natl. Acad. Sci. U. S. A. 110, 7856–7861. https://doi.org/10.1073/pnas.1220823110

Okamoto, A., Nakamura, R., Hashimoto, K., 2011. Electrochim. Acta 56, 5526–5531. https://doi.org/10.1016/j.electacta.2011.03.076

Okamoto, A., Nakamura, R., Nealson, K.H., Hashimoto, K., 2014. ChemElectroChem 1, 1808–1812. https://doi.org/10.1002/celc.201402151

430 Robertson, I.B., Stevens, J.M., Ferguson, S.J., 2008. FEBS Lett. 582, 3067–3072.
431 https://doi.org/10.1016/j.febslet.2008.07.052
432 Rosenbaum, M.A., Bar, H.Y., Beg, Q.K., Segrè, D., Booth, J., Cotta, M.A., Angenent, L.T., 2012. PLoS
433 One 7, e30827. https://doi.org/10.1371/journal.pone.0030827
434 Sanders, C., Turkarslan, S., Lee, D.-W., Daldal, F., 2010. Trends Microbiol. 18, 266–274.
435 https://doi.org/10.1016/j.tim.2010.03.006
436 Santoro, C., Arbizzani, C., Erable, B., Ieropoulos, I., 2017. J. Power Sources 356, 225–244.
437 https://doi.org/10.1016/j.jpowsour.2017.03.109
438 Schmitz, S., Nies, S., Wierckx, N., Blank, L.M., Rosenbaum, M.A., 2015. Front. Microbiol. 6, 284.
439 https://doi.org/10.3389/fmicb.2015.00284
440 Schuergers, N., Werlang, C., Ajo-Franklin, C.M., Boghossian, A.A., 2017. Energy Environ. Sci. 10,
441 1102–1115. https://doi.org/10.1039/C7EE00282C
442 Sekar, N., Jain, R., Yan, Y., Ramasamy, R.P., 2016. Biotechnol. Bioeng. 113, 675–679.
443 https://doi.org/10.1002/bit.25829
444 Shi, L., Dong, H., Reguera, G., Beyenal, H., Lu, A., Liu, J., Yu, H.-Q., Fredrickson, J.K., 2016. Nat. Rev.
445 Microbiol. 14, 651–662. https://doi.org/10.1038/nrmicro.2016.93
446 Shi, L., Richardson, D.J., Wang, Z., Kerisit, S.N., Rosso, K.M., Zachara, J.M., Fredrickson, J.K., 2009.
447 Environ. Microbiol. Rep. 1, 220–227. https://doi.org/10.1111/j.1758-2229.2009.00035.x
448 Slate, A.J., Whitehead, K.A., Brownson, D.A.C., Banks, C.E., 2019. Renewable Sustainable Energy Rev.
449 101, 60–81. https://doi.org/10.1016/j.rser.2018.09.044
450 Sturm-Richter, K., Golitsch, F., Sturm, G., Kipf, E., Dittrich, A., Beblawy, S., Kerzenmacher, S.,
451 Gescher, J., 2015. Bioresour. Technol. 186, 89–96. https://doi.org/10.1016/j.biortech.2015.02.116
452 Su, L., Ajo-Franklin, C.M., 2019. Curr. Opin. Biotechnol. 57, 66–72.
453 https://doi.org/10.1016/j.copbio.2019.01.018
454 Su, L., Fukushima, T., Prior, A., Baruch, M., Zajdel, T.J., Ajo-Franklin, C.M., 2020. ACS Synth. Biol. 9,
455 115–124. https://doi.org/10.1021/acssynbio.9b00379

456 Sun, Y.-L., Tang, H.-Y., Ribbe, A., Duzhko, V., Woodard, T.L., Ward, J.E., Bai, Y., Nevin, K.P.,
457 Nonnenmann, S.S., Russell, T., Emrick, T., Lovley, D.R., 2018. Small 14, e1802624.
458 https://doi.org/10.1002/smll.201802624
459 TerAvest, M.A., Zajdel, T.J., Ajo-Franklin, C.M., 2014. ChemElectroChem 1, 1874–1879.
460 https://doi.org/10.1002/celc.201402194
461 Thirumurthy, M.A., Jones, A.K., 2020. Nanotechnology 31, 124001. https://doi.org/10.1088/1361-
462 6528/ab5de6
463 Thöny-Meyer, L., 2000. Biochim. Biophys. Acta 1459, 316–324. https://doi.org/10.1016/s0005-
464 2728(00)00167-5
465 Verissimo, A.F., Yang, H., Wu, X., Sanders, C., Daldal, F., 2011. J. Biol. Chem. 286, 40452–40463.
466 https://doi.org/10.1074/jbc.M111.277764
467 Wang, F., Gu, Y., O'Brien, J.P., Yi, S.M., Yalcin, S.E., Srikanth, V., Shen, C., Vu, D., Ing, N.L.,
468 Hochbaum, A.I., Egelman, E.H., Malvankar, N.S., 2019. Cell 177, 361–369.
469 https://doi.org/10.1016/j.cell.2019.03.029
470 Wang, X., Gao, N., Zhou, Q., 2013. Biosens. Bioelectron. 43, 264–267.
471 https://doi.org/10.1016/j.bios.2012.12.029
472 Webster, D.P., TerAvest, M.A., Doud, D.F.R., Chakravorty, A., Holmes, E.C., Radens, C.M., Sureka, S.,
473 Gralnick, J.A., Angenent, L.T., 2014. Biosens. Bioelectron. 62, 320–324.
474 https://doi.org/10.1016/j.bios.2014.07.003
475 West, E.A., Jain, A., Gralnick, J.A., 2017. ACS Synth. Biol. 6, 1627–1634.
476 https://doi.org/10.1021/acssynbio.6b00349
477 Xu, S., Jangir, Y., El-Naggar, M.Y., 2016. Electrochim. Acta 198, 49–55.
478 https://doi.org/10.1016/j.electacta.2016.03.074
479 Yang, Y., Zhou, H., Mei, X., Liu, B., Xing, D., 2018. Front. Microbiol. 9, 1924.
480 https://doi.org/10.3389/fmicb.2018.01924
481 Zajdel, T.J., Baruch, M., Méhes, G., Stavrinidou, E., Berggren, M., Maharbiz, M.M., Simon, D.T., Ajo-

Franklin, C.M., 2018. Sci. Rep. 8, 15293. https://doi.org/10.1038/s41598-018-33521-9

Zheng, X.-M., Hong, J., Li, H.-Y., Lin, D.-H., Hu, H.-Y., 2012. Biochim. Biophys. Acta 1824, 1394–1400. https://doi.org/10.1016/j.bbapap.2012.06.017

Zhou, A.Y., Baruch, M., Ajo-Franklin, C.M., Maharbiz, M.M., 2017. PLoS One 12, e0184994. https://doi.org/10.1371/journal.pone.0184994